Kinematics and deformation of the southern Red Sea region from GPS observations

Renier Viltres, Sigurjón Jónsson, Joël Ruch, Cécile Doubre, Robert Reilinger, Michael Floyd, Ghebrebrhan Ogubazghi

HAL Id: insu-03707760

https://insu.hal.science/insu-03707760

Submitted on 29 Jun 2022

Kinematics and deformation of the southern Red Sea region from GPS observations

Renier Viltres [1], Sigurjón Jónsson,[1] Joël Ruch,[1,2] Cécile Doubre,[3] Robert Reilinger,[4] Michael Floyd [4] and Ghebrebrhan Ogubazghi[5]

[1]*King Abdullah University of Science and Technology (KAUST), Physical Science and Engineering Division (PSE), Thuwal 23955-6900, Saudi Arabia.*
E-mail: renier.ladrondeguevara@kaust.edu.sa
[2]*Department of Earth Sciences, University of Geneva, Geneva 1205, Switzerland*
[3]*Institut de Physique du Globe de Strasbourg, UMR 7516, Université de Strasbourg/EOST, CNRS, 5 rue René Descartes, F-67084 Strasbourg Cedex, France*
[4]*Department of Earth, Atmospheric, and Planetary Sciences, Massachusetts Institute of Technology, Cambridge, MA 02139, USA*
[5]*Department of Earth Sciences, Eritrea Institute of Technology, Asmara 12676, Eritrea*

SUMMARY

The present-day tectonics of the southern Red Sea region is complicated by the presence of the overlapping Afar and southern Red Sea rifts as well as the uncertain kinematics and extent of the Danakil block in between. Here we combine up to 16 yr of GPS observations and show that the coherent rotation of the Danakil block is well described by a Danakil-Nubia Euler pole at 16.36°N, 39.96°E with a rotation rate of 2.83 deg Myr^{-1}. The kinematic block modeling also indicates that the Danakil block is significantly smaller than previously suggested, extending only to Hanish-Zukur Islands (∼13.8°N) with the area to the south of the islands being a part of the Arabian Plate. In addition, the GPS velocity field reveals a wide inter-rifting deformation zone across the northern Danakil-Afar rift with ∼5.6 mm yr^{-1} of east–west opening across Gulf of Zula in Eritrea. Together the results redefine some of the plate boundaries in the region and show how the extension in the southern Red Sea gradually moves over to the Danakil-Afar rift.

Key words: Plate motions; Satellite geodesy; Time-series analysis; Continental margins: divergent.

1 INTRODUCTION

The tectonics in Afar and its surrounding regions of the southern Red Sea and Gulf of Aden is dominated by the Arabia–Nubia–Somalia ridge–ridge–ridge triple junction. It is the only place on Earth allowing for inland observations of all evolution stages of a divergent plate boundary: from the continental rifting to the onset of an oceanic ridge (e.g. Wolfenden *et al.* 2005; Stab *et al.* 2016; Varet 2018). This makes the region a unique location to study divergent plate kinematics and processes of microplate formation in a young and active triple junction (Eagles *et al.* 2002; Schettino *et al.* 2016; Doubre *et al.* 2017).

The Oligocene to present tectonic evolution of the triple junction has involved several phases of spreading-centre reorganization that have led to the formation and isolation of microplates (Cochran 1983; Courtillot *et al.* 1987; Acton *et al.* 1991; Manighetti *et al.* 2001a; Bosworth 2015), similar to what has been observed at other divergent plate boundaries like the East Pacific Rise and the Pacific–Nazca–Antarctic triple junction (Anderson-Fontana *et al.* 1986; Engeln *et al.* 1988). The Danakil and Ali-Sabieh blocks are examples of such isolated continental microplates (Fig. 1), associated with

the propagation of the Red Sea and Gulf of Aden rifts into Afar (Le Pichon & Francheteau 1978; Courtillot *et al.* 1984; Garfunkel & Beyth 2006).

Several studies have focused on the plate kinematics of the southern Red Sea region over the past decades (e.g. Chu & Gordon 1998; Collet *et al.* 2000; Eagles *et al.* 2002; McQuarrie *et al.* 2003; Ar-Rajehi *et al.* 2010; McClusky *et al.* 2010; Reilinger & McClusky 2011; McQuarrie & van Hinsbergen 2013; Schettino *et al.* 2016; Doubre *et al.* 2017). However, the present-day plate boundary configuration and the relative plate motions are still not well resolved for the entire area (Schettino *et al.* 2016). The main difficulties include (1) that the plate boundary deformation is broadly distributed over hundreds of kilometres rather than being focused at sharp boundaries (CNR & CNRS 1975; Hayward & Ebinger 1996), (2) that parts of the Nubia–Arabia Plate boundary in the Red Sea are buried under thick salt deposits (Frazier 1970; Carbone *et al.* 1998), (3) that small transform fault offsets (less than 5 km) along with incipient structures characterize the Red Sea spreading centre and the Nubia–Arabia–Somalia Plate boundaries, respectively (Chu & Gordon 1998; Ebinger *et al.* 2010), (4) lack of continuous geodetic observations (particularly in Yemen) and (5) that many tectonic
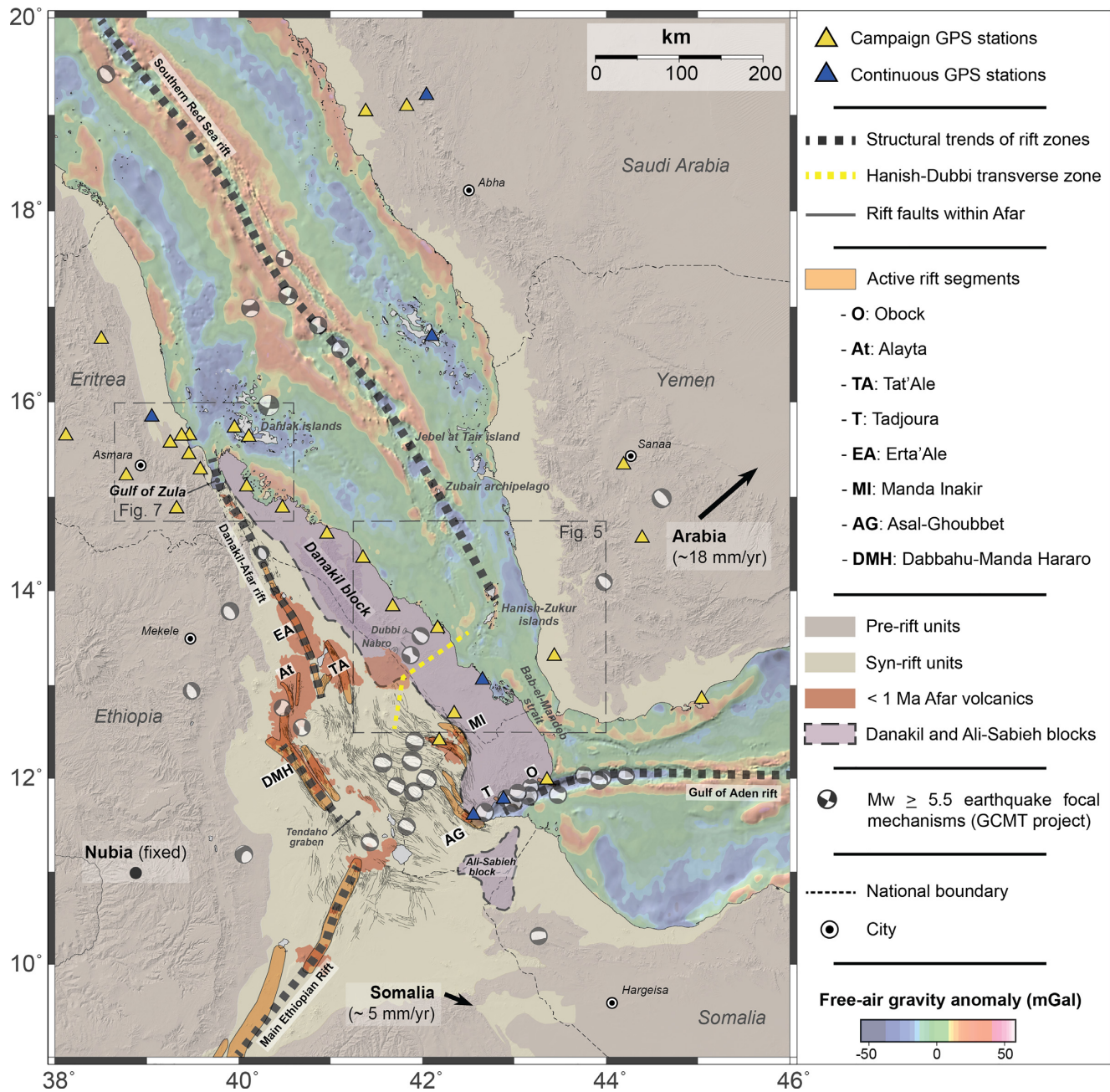
Figure 1. Tectonic settings of the southern Red Sea, Afar and Gulf of Aden region. Major active rift segments defined after Manighetti *et al.* (1998) and Pagli *et al.* (2014) and the Hanish-Dubbi transverse zone after Barberi & Varet (1977) and Varet (2018). Background hillshaded topography and bathymetry from [http://topex.ucsd.edu/] and offshore free-air gravity anomalies (version 27) from Sandwell *et al.* (2014).

structures within Afar are covered by young (∼1–4 Ma) volcanic deposits (Barberi & Varet 1977; Acton *et al.* 1991).

In addition, the mechanisms controlling the plate kinematics in the region appear to be scale-dependent (Manighetti *et al.* 2001a): While large- and regional-scale (100–1000 km) deformation is well described by steady-state rotation of rigid lithospheric blocks (McKenzie *et al.* 1970; Acton *et al.* 1991; Chu & Gordon 1998; Eagles *et al.* 2002; McClusky *et al.* 2010; Saria *et al.* 2013; Schettino *et al.* 2016; Altamimi *et al.* 2017; Doubre *et al.* 2017), the crust beneath Afar is too dissected by faulting and magmatic intrusions for rigidity concepts to apply at smaller (∼10 km) spatial scales (Makris & Ginzburg 1987; Ebinger & Hayward 1996; Bastow & Keir 2011).

Adding to the complex tectonic settings of the region, the southern Red Sea rift steps on land south of ∼17°N, progressively transferring the Nubian–Arabian extension over to the Danakil-Afar rift, which consists of several active spreading centres, e.g., Erta'Ale, Tat'Ali, Alayta and Dabbahu-Manda Hararo (Mohr 1970; Tazieff *et al.* 1972; Barberi & Varet 1977; Tapponnier *et al.* 1990; Beyth 1991; Keir *et al.* 2013; Doubre *et al.* 2017, Fig. 1). The southern Red Sea rift continues south of 17°N to Zubair Islands (∼15°N) and Hanish-Zukur Islands (∼13.8°N), and possibly all the way through Bab-el-Mandeb Strait connecting to the Gulf of Aden rift (Mohr 1970; McKenzie *et al.* 1970; Schettino *et al.* 2016). The overlapping southern Red Sea and Danakil-Afar rifts define a ∼600-km-long and ∼200-km-wide zone of unstretched crust (Fig. 1), that is
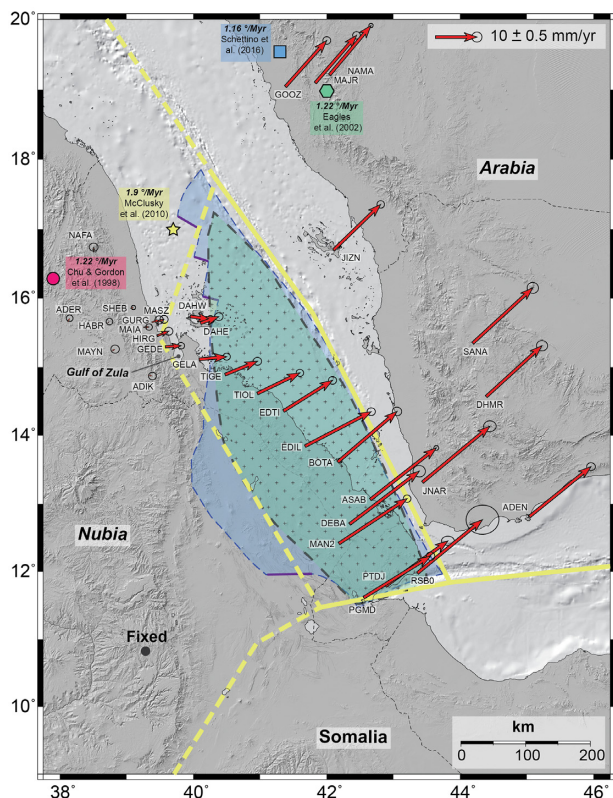
Figure 2. Horizontal GPS velocities for the time period 2001–2016 with respect to Nubia (with 95 per cent confidence ellipses). The spatial extent of the Danakil block in different microplate models is shown by the green (Chu & Gordon 1998; Eagles *et al.* 2002), yellow (McClusky *et al.* 2010) and blue (Schettino *et al.* 2016) polygons as well as the Danakil-Nubia Euler pole locations of these models.

the so-called Danakil block (Manighetti *et al.* 1998). The differential motions between the two rift branches are fully accommodated by rigid rotation of the block (Mohr 1970; Le Pichon & Francheteau 1978), and therefore, its kinematics is key for the overall Nubia–Arabia relative divergence (Varet 2018). Models aiming to describe the present-day kinematics of the Danakil block include progressive tearing (Courtillot 1980), 'crank-arm' tectonics (Sichler 1980; Souriot & Brun 1992; Collet *et al.* 2000) and microplate models (Barberi & Varet 1977; Acton *et al.* 1991; Eagles *et al.* 2002; Mc-Clusky *et al.* 2010; Schettino *et al.* 2016) that consider rigid rotation of the block about a single Euler pole (Fig. 2).

McClusky *et al.* (2010) pioneered using GPS observations to constrain the present-day kinematics of the Danakil block. Their model used a single Euler pole (17.0°N; 37.9°E; rate: 1.9 deg Myr⁻¹) for the Danakil-Nubia relative motions, in line with earlier microplate models (Fig. 2). A plate reconstruction about this pole resulted in a microplate age of ∼9.3 Ma, but involved substantial overlap of unextended terrain along the northern part of the Danakil block. They suggested that this overlap implied a northward migration of the Euler pole of ∼200 km to its current location since the isolation of the Danakil microplate. Following this suggestion, Reilinger & McClusky (2011) estimated an initiation of opening of Gulf of Zula at ∼5 Ma and initial separation of the Danakil block from Nubia at 11 ± 2 Ma. The results from Schettino *et al.* (2016) also indicate migration of the Danakil-Nubia Euler pole (∼390 km since 4.6 Ma), although their plate boundary configuration and Euler pole

migration history differs from those in McClusky *et al.* (2010) and Reilinger & McClusky (2011) (Fig. 2).

In this study, we use GPS observations acquired in March 2016 to extend GPS position time-series resulting in an improved velocity field for the southern Red Sea region. From the velocity field, we analyse the present-day kinematics of the Danakil block, for example by revisiting the kinematic block-modeling approach of McClusky *et al.* (2010), and report on active deformation near the Gulf of Zula in northern Eritrea. After describing shortcomings of earlier kinematic block models, we propose an alternative model where the southernmost part of the Red Sea is considered as a part of the Arabian plate.

2 GPS DATA PROCESSING

We analysed GPS data from both continuous/permanent stations and measurement campaigns within our study area collected during the period 2001–2016 (Fig. 2). Most stations and survey sites were installed by the MIT, the Eritrea Institute of Technology (data available at Ghebreab *et al.* 2010a,b; Ogubazghi & Reilinger 2010a,b,c,d; ArRajehi *et al.* 2013) and the French mobile network (data available at [https://gnsscope.dt.insu.cnrs.fr/spip/]) in the early 2000s and the survey sites have been measured several times since then. In March 2016 we re-occupied all the Saudi Arabian and Eritrea GPS sites (except DEBA), extending the observations at 19 locations. A similar data set exists for the GPS locations in Djibouti and Ethiopia, but no observations have been made at the Yemeni GPS sites since 2008. The updated data set doubles the time span covered by Mc-Clusky *et al.* (2010) and includes observations from four new sites (BOTA, MAN2, DAHE, DAHW, Fig. 2, Table 1.

We used the GAMIT/GLOBK software (Herring *et al.* 2015) to analyse the GPS data and followed the approach described by Floyd *et al.* (2010) and Kogan *et al.* (2012). A total of 18 IGS core stations were added to the processing in order to estimate a consistent transformation (translation and rotation) stabilizing our network to the ITRF2008 reference frame (Altamimi *et al.* 2012). We then combined daily solutions for each continuous GPS station and survey site into position time-series, leading to a set of velocities with respect to ITRF2008. Angular velocities from the Altamimi *et al.* (2012) plate motion model were used to rotate the velocity field into a Nubian-fixed reference frame (Fig. 2). To estimate realistic uncertainties for the GPS velocities, we included the character of the time-series noise in the analysis (see Floyd *et al.* (2010) for details), which yielded horizontal velocity component uncertainties of <0.5 mm yr⁻¹ for most of the survey sites.

Prior to the GPS velocity estimation, we checked each position time-series for possible changes associated with the volcano-tectonic events that occurred in the area during the observation period. In particular, we checked for possible response to the 2004 Dallol dyke intrusion (Nobile *et al.* 2012), the 2005–2010 Dabahu-Manda Harraro rifting episode (Wright *et al.* 2006; Grandin *et al.* 2009; Hamling *et al.* 2010), the 2008 Alu-Dalafilla volcanic eruption (Pagli *et al.* 2012), the 2007 Jebel at Tair and 2011–2013 Zubair islands eruptions (Xu & Jónsson 2014; Xu *et al.* 2015), the 2010–2011 Gulf of Aden rifting episode (Ahmed *et al.* 2016) and the 2011 Nabro volcanic eruption (Hamlyn *et al.* 2014; Goitom *et al.* 2015). None of the position times-series show significant rate changes that correspond to these events nor to post-dyking deformation in the area (e.g. Doubre *et al.* 2017), except those of the southernmost stations PGMD, PTDJ and RSB0 (Fig. 2). These stations are located on the northern margins of the active Asal-Ghoubbet, Tadjoura and

Table 1. Horizontal GPS velocities with respect to the Nubian plate.

Site	Lon. (°)	Lat. (°)	Ve (mm yr^{-1})	Vn (mm yr^{-1})	σVe (mm yr^{-1})	σVn (mm yr^{-1})	Rho
ADEN	45.040	12.812	14.85	12.03	0.43	0.39	− 0.006
ADER	38.119	15.655	0.46	0.93	0.33	0.32	− 0.004
ADIK	39.325	14.883	1.02	− 0.23	0.39	0.37	− 0.000
ASAB	42.654	13.063	15.90	12.43	0.24	0.24	0.000
BOTA	42.167	13.614	14.29	12.20	0.46	0.42	− 0.039
DAHE	40.110	15.639	4.40	1.58	0.41	0.39	− 0.007
DAHW	39.955	15.737	4.88	− 0.74	0.40	0.38	− 0.008
DEBA	42.346	12.703	16.76	12.73	0.61	0.57	− 0.017
DHMR	44.392	14.571	13.46	12.26	0.55	0.51	− 0.017
EDIL	41.677	13.845	15.95	8.33	0.41	0.38	− 0.002
EDTI	41.353	14.359	11.82	7.40	0.40	0.38	− 0.011
GEDE	39.583	15.296	3.77	0.25	0.35	0.32	− 0.007
GELA	40.088	15.114	6.65	0.63	0.36	0.34	0.002
GOOZ	41.383	19.042	9.95	11.14	0.39	0.37	− 0.007
GURG	39.465	15.657	1.55	0.63	0.40	0.39	− 0.009
HABR	38.715	15.638	0.46	0.40	0.33	0.32	0.005
HIRG	39.458	15.456	2.80	1.09	0.41	0.39	− 0.006
JIZN	42.104	16.699	11.37	10.99	0.37	0.37	− 0.001
JNAR	43.436	13.317	16.27	13.51	0.62	0.53	0.004
MAIA	39.255	15.578	1.31	0.08	0.33	0.32	− 0.003
MAJR	41.829	19.096	9.95	11.47	0.38	0.37	− 0.003
MAN2	42.184	12.416	16.44	10.82	0.38	0.36	− 0.004
MASZ	39.379	15.652	1.77	0.57	0.41	0.40	− 0.010
MAYN	38.776	15.233	0.84	0.48	0.42	0.40	− 0.011
NAFA	38.504	16.670	0.04	1.17	0.44	0.40	− 0.017
NAMA	42.045	19.211	9.97	11.89	0.21	0.21	0.004
PGMD	42.556	11.617	16.12	10.01	0.42	0.42	0.003
PTDJ	42.884	11.789	15.02	10.89	0.63	0.46	− 0.002
RSB0	43.362	11.980	15.67	12.88	1.62	1.44	0.010
SANA	44.190	15.348	14.48	13.35	0.56	0.54	− 0.027
SHEB	39.054	15.853	0.80	0.22	0.21	0.21	0.000
TIGE	40.477	14.891	7.81	3.22	0.41	0.39	− 0.006
TIO1	40.961	14.615	10.26	4.98	0.37	0.35	− 0.029

Obock rift segments (Fig. 1), associated with the inland propagation of the Aden Ridge into Afar (Manighetti *et al.* 1998; Doubre *et al.* 2017). Moreover, the observed velocity change at RSB0 (near the Obock rift segment, Fig. 1), which occurred about a year before the 2010–2011 Gulf of Aden rifting episode (Ahmed *et al.* 2016), was also identified by Doubre *et al.* (2017) and remains poorly understood. Therefore, we suggest that the three stations are affected by some transient motion and we removed the affected parts of the position time-series to ensure that the estimated velocities represent the steady-state motion at these locations.

3 GPS VELOCITY FIELD

Estimated velocities relative to the Nubian plate along with their 95 per cent confidence ellipses are shown in Fig. 2 (see also Table 1). The Euler vectors between the ITRF08 and major tectonic plates in the area (Arabia, Nubia and Somalia) were defined after the Altamimi *et al.* (2012) plate-motion model due to the limited number of stations outside the Danakil block. GPS stations located in stable Nubia (west of station MAIA, Fig. 2) show small residual velocities below 0.6 mm yr^{-1}, indicating that our solution is broadly consistent with the Altamimi *et al.* (2012) plate-motion model. Likewise, the estimated velocities at GPS stations within the Arabian plate match the predicted motions (∼18.0 mm yr^{-1} at ∼14.6°N and ∼ 14.5 mm yr^{-1} at ∼19.0°N) by their Arabia–Nubia Euler vector. In contrast, GPS stations located along the Eritrean

coast (Fig. 2) show motions that deviate from the large-scale rigid plate model of Altamimi *et al.* (2012).

At least four sites in the north of our GPS network (GEDE, HIRG, GURG, MASZ) show small but significant motions towards Gulf of Zula (Fig. 2). These departures from the Nubian-fixed reference frame suggest elastic inter-rifting coupling of the plate boundary (Joffe & Garfunkel 1987; Vigny *et al.* 2006; Smittarello *et al.* 2016), with a clear east–west velocity gradient across the gulf, consistent with present-day opening motions across the Zula-Bada corridor (Frazier 1970, Fig. 2). Further evidence for plate divergence and active rifting in the area is provided by well-exposed extensional structures (e.g. Sani *et al.* 2017) and recent seismic activity (e.g. Illsley-Kemp *et al.* 2018) throughout the area.

From the Dahlak islands in the northwest (Fig. 1), the GPS velocities increase towards southeastern Eritrea and Djibouti, where they equal the observed rates in stable Arabia (Fig. 2). Similar GPS velocities of ∼20 mm yr^{-1} towards ∼N53°E on both sides of the Bab-el-Mandeb Strait (Fig. 2), in addition to the suggested termination of the southern Red Sea ridge at ∼14.8°N (Barberi & Varet 1977; Schettino *et al.* 2016; Varet 2018) or at Hanish-Zukur Islands (∼13.8°N, Fig. 1), indicate no significant opening motions across the southernmost Red Sea at present (also suggested by Vigny *et al.* 2006, 2007; Doubre *et al.* 2017) and thus a full transfer of extension from the southern Red Sea rift into the subaerial Danakil-Afar rift. The increase of the station velocities toward southeast is also consistent with that expected from a small rigid block rotating around a near-by Euler pole (Acton *et al.* 1991), supporting the microplate

models (e.g. Chu & Gordon 1998; Eagles *et al.* 2002; McClusky *et al.* 2010; Schettino *et al.* 2016).

4 RIGID BLOCK MODEL

In this section, we use our improved GPS velocity field in and around the Danakil block and revisit the block-rotation model of McClusky *et al.* (2010). As previously mentioned, our velocity field is based on longer GPS time-series than in the previous study and includes four new stations at both the northern (DAHE, DAHW) and southern end of the Danakil block (DEBA, MAN2, Fig. 2) operating in the area since late 2007. In addition, we integrated results from recent studies (e.g. Doubre *et al.* 2017; Sani *et al.* 2017; Illsley-Kemp *et al.* 2018) in defining the Danakil block boundaries used in our kinematic model. The software package Tdefnode (McCaffrey 1995, 2002, 2009) was used for all the elastic block modeling presented hereafter. It allows for relative motions between rigid blocks to be specified by poles of rotation and node sets defining block boundaries. Model parameters as angular velocities are estimated by least-squares fit to the GPS data. Similar to former studies (e.g. Eagles *et al.* 2002; McClusky *et al.* 2010; Schettino *et al.* 2016), our regional-scale kinematic model assumes rigid blocks with free-slipping block boundaries.

We begin by comparing our updated GPS velocity field to the velocities predicted by the block model of McClusky *et al.* (2010), which we term as Model 1. The residual velocities near the southern edge of the Danakil block (south of ~12°N, stations PGMD, PTDJ, RSB0) show a systematic rate overestimation in the EW direction (Fig. 3a). In contrast, velocities at stations located further north between ~12°N and 14.5°N appear to require a higher block-rotation rate than Model 1 predicts. Velocities at the new stations in the Dahlak islands (DAHE and DAHW) and station GELA are, on the other hand, well described by the model (Fig. 3a), suggesting that the block boundary is effectively further west than the one proposed by Eagles *et al.* (2002) and Schettino *et al.* (2016, Fig. 2).

Before re-estimating the Danakil–Nubia angular velocity using our new GPS velocity field, we slightly modified the Danakil block boundaries of Model 1 (McClusky *et al.* 2010) by integrating results from several other studies (here termed as Model 2). The southernmost boundary was defined after the Doubre *et al.* (2017) block model for Central Afar, constrained by dense and recent geodetic measurements in the area. It follows the en echelon segments of the Aden ridge (Obock, Tadjoura and Asal-Ghoubbet, Fig. 1) and continues westward until the southeastern border of the Tendaho graben (Fig. 1). The Doubre *et al.* (2017) block model includes a northwest continuation of this boundary (dashed-brown line in Fig. 3b) connecting the Tendaho graben with the recently activated Dabbahu–Manda–Hararo rift segment. This continuation has been proposed as the westernmost Danakil–Nubia boundary at present (e.g. Bird 2003; Schettino *et al.* 2016), with seismic activity in the area (e.g. Illsley-Kemp *et al.* 2018) illuminating its path towards the Danakil Depression (dashed-purple line in Fig. 3b). However, the GPS data in this area do not provide reliable information on the steady-state motion of the plates, due to the co- and post-dyking deformation caused by the 2005–2010 Dabbahu-Manda Hararo rifting episode, associated with several metres of horizontal displacement (Wright *et al.* 2006; Grandin *et al.* 2009; Hamling *et al.* 2010; Pagli *et al.* 2014; Doubre *et al.* 2017). Therefore, we defined the Danakil–Nubia western boundary along the central Danakil Depression, similar to McClusky *et al.* (2010). Further north in the Gulf

of Zula area, the boundary of Model 2 follows earthquake locations from recent seismicity (Illsley-Kemp *et al.* 2018) and runs roughly parallel to the mean strike orientation of tectonic structures in the area (e.g. Sani *et al.* 2017, Fig. 3b). North of Dahlak Islands the plate-boundary location of Bird (2003) correlates well with both earthquakes offshore Massawa and strike-slip focal mechanisms close to the ridge axis (McKenzie *et al.* 1970, Fig. 1). Thus, we located the northernmost block boundary segment of Model 2 using the above references.

Using our improved GPS velocities and updated block boundaries, the Model 2 yields almost identical angular velocity results as for Model 1 when using the same set of Danakil GPS stations. However, when excluding the three southernmost sites, the estimated pole location moves ~42 km to the south from the previous estimate (Model 2, 16.62°N, 39.73°E) and the angular rotation rate is 21 per cent higher (2.3 deg Myr^{-1}) than for Model 1. Albeit balanced by the southward location of the Euler pole in Model 2 relative to Model 1, the higher rotation rate decreases the residual velocity WRMS error for GPS stations located north of ~12°N by 26 per cent. Yet, the residual velocity map still shows the same change in polarity north and south of GPS station ASAB, with the model underpredicting observed velocities in central Danakil while slightly overpredicting the two velocities just south of ASAB (Fig. 3b). One explanation for the specific behaviour of the three southernmost stations could be elastic coupling at the trans-tensional Gulf of Aden plate boundary. However, GPS studies focusing on Djibouti have concluded that the elastic coupling at these locations is limited (e.g. Vigny *et al.* 2006; Doubre *et al.* 2017). Therefore, the updated velocity field may rather suggest the two regions north and south of ASAB are moving independently of each other. Furthermore, the compression the models predict across Bab-el-Mandeb Strait is not compatible with the kinematics of the southern Red Sea (Manighetti *et al.* 1997; Schettino *et al.* 2016) as well as with the limited differential motions in our updated velocity field and in those from previous studies (e.g. Vigny *et al.* 2006, 2007; McClusky *et al.* 2010; Doubre *et al.* 2017).

5 ALTERNATIVE BLOCK MODEL

The shortcomings of Models 1 and 2 and the somewhat different behaviour of the northern and southern Danakil GPS stations suggest the need for more than one Euler vector in explaining the current motions of the entire Danakil region (Barberi & Varet 1977; Courtillot 1982). In line with this, the suggested termination of the southern Red Sea rift at ~14.8°N (Schettino *et al.* 2016) or at Hanish-Zukur Islands (~13.8°N) and the absence of seismic activity in Bab-el-Mandeb Strait (Al-Amri *et al.* 1998, fig. 1) have been related to a possible connection between the southern Red Sea and Danakil-Afar rifts via the so-called Hanish-Dubbi transverse zone (Barberi & Varet 1977; Varet 2018, Fig. 1). Here we test whether or not the updated velocity field supports such a plate-boundary configuration.

Our alternative block model configuration (Model 3) considers the Hanish-Zukur volcanic islands as the southeastern edge of the Danakil block. Differently from the Bab-el-Mandeb Strait, seismic activity in the area between the Zubair and Hanish-Zukur groups (e.g. Hofstetter & Beyth 2003; ISC 2019) is consistent with an active plate boundary along this portion of the Southern Red Sea axis (Varet 2018). The block boundary configuration is
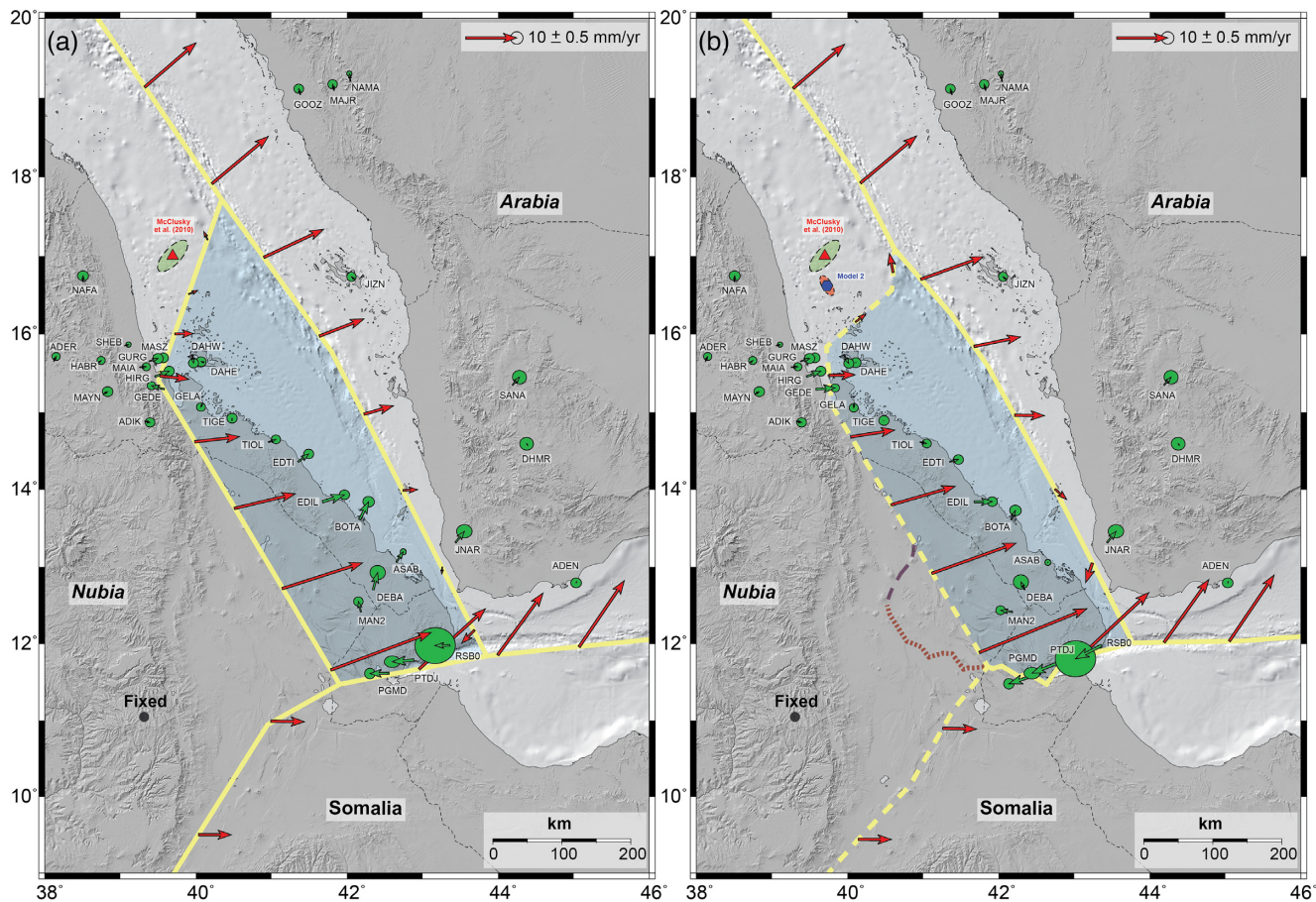
Figure 3. Results for Models 1 (a) and 2 (b) using our updated GPS velocity field. Yellow lines mark block boundaries (dashed lines show less certain boundary locations), green arrows show residual GPS velocities (with 95 per cent confidence ellipses), and red arrows indicate predicted model velocities at the block boundaries (reference block is to the west/south). Red triangle and blue hexagon depict the Danakil-Nubia Euler pole from McClusky *et al.* (2010) and Model 2 (stations PGMD, PTDJ and RSB0 were excluded in the estimation), respectively. Likewise, dashed brown and purple lines show the southwestern Danakil block boundary according to Doubre *et al.* (2017) and lineations of recent seismicity (e.g. Illsley-Kemp *et al.* 2018).

further supported by the clear N40°E alignment of volcanic landforms within the islands, numerous submarine volcanic vents to the southwest and the island group itself (e.g. Gass *et al.* 1973), all located along a band of high magnetic anomalies (Fig. 4). Although similar well-expressed structures are absent within Afar (e.g. Varet 2018), the Nabro and the Dubbi volcanoes strike almost parallel to the Hanish-Zukur islands and are important geomorphological markers crossing the Danakil block. These volcanoes locate along transverse alignments in the area (e.g. Hanish-Dubbi, Fig. 1), which have been proposed to represent the surface expression of a NE–SW oriented 'leaky' transform fault, allowing for spreading segments within Afar to totally replace the oceanic Red Sea rift zone (Barberi & Varet 1977). Considering the information above, we defined the southernmost Danakil block boundary from the Hanish-Zukur volcanic lineations (Fig. 4) and in such a way that presently stabilized margins within Afar (defined after Varet 2018) remain parts of the Arabian plate (Fig. 5). The less constrained on land segment of this boundary minimizes predicted compressional motions towards the Danakil Depression while remaining broadly consistent with zones of separation between different crustal domains (inferred from *S*-wave seismic tomography, for example, Guidarelli *et al.* 2011; Hammond *et al.* 2014) and high shear strain rates determined from InSAR (e.g. Pagli *et al.*

2014). The rest of the block boundaries are the same as in Model 2 (Fig. 5).

The results of the angular velocity optimization for Model 3 are presented in Fig. 5 (see also Table 2) as residual velocities and predicted relative motions between interacting tectonic plates. As expected from the GPS velocity residuals of Models 1 and 2 north of Hanish-Zukur Islands, the modeling here results in a higher angular rotation rate (2.83 deg Myr^{-1}) for the Danakil-Nubia relative motion, an increase that is also due to the ∼38 km southward shift of the pole position (16.36°N, 39.96°E). The predicted velocities by Model 3 explain the GPS data north of station ASAB with a 53 and 36 per cent WRMS error reduction relative to Model 1 and 2, respectively (Fig. 5). Likewise, GPS velocities at stations located to the south of the Danakil block are better described by the Arabia–Nubia Euler vector (defined after Altamimi *et al.* 2012), for which the WRMS error of Model 3 is reduced by 39 per cent and 49 per cent compared to Models 1 and 2. Four stations across the Bab-el-Mandeb Strait (ASAB, DEBA, JNAR, MAN2, Fig. 5) show residual velocities of ∼2 mm yr^{-1} towards ∼N45°E, confirming for null differential motions in the area at present. A possible explanation for these departures from the frame realization may be that the angular velocity of the Arabian plate in the Altamimi *et al.* (2012) plate motion model is constrained by only four GPS stations,
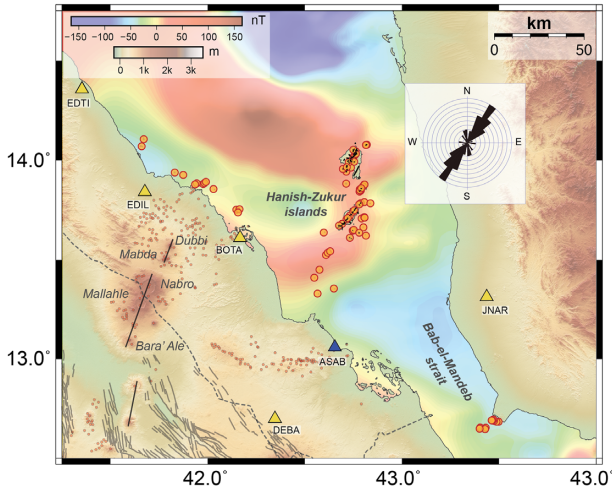
Figure 4. Offshore volcanic vents (orange circles) and alignments (black lines) in and near Hanish-Zukur Islands. The rose diagram shows the dominating strike of vent alignments, crater elongations, eruptive fissures and/or volcanic ridges in the area (all structures were mapped in Google Earth). Several volcanoes in the Nabro volcanic area are labeled and inland volcanic vent locations are highlighted by red dots. Continuous GPS stations and survey sites are depicted by blue and yellow triangles, respectively. Marine-satellite magnetic anomalies after (Maus *et al.* 2009).
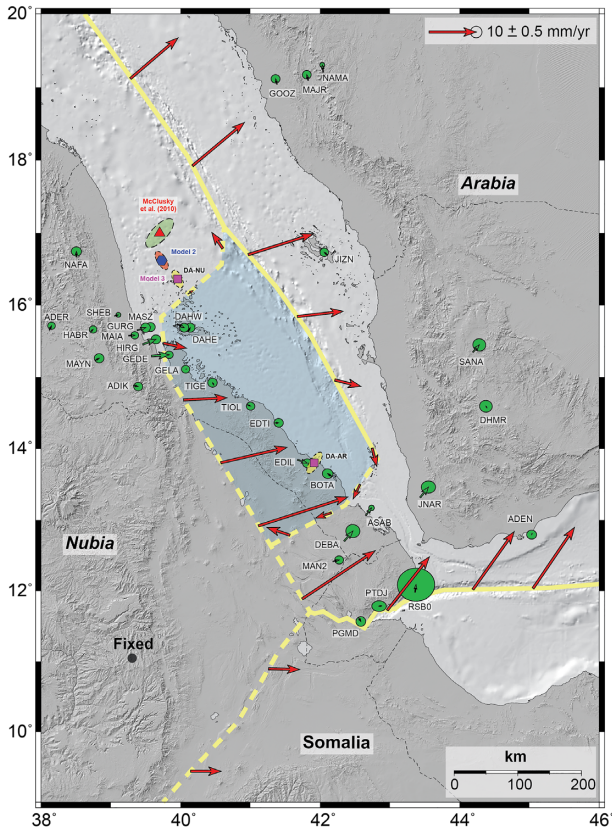

Figure 5. Results for Model 3 with a smaller Danakil block. The Danakil-Nubia (DA-NU) and Danakil-Arabia (DA-AR) Euler poles of relative motion are shown by purple squares. Yellow lines mark block boundary locations (dashed yellow lines show less certainty boundaries), green arrows show residual GPS velocities (with 95 per cent confidence ellipses), and red arrows show model-predicted velocities at block boundaries (reference block is to the west/south).

differently from the Nubian plate, for which 11 stations were used. In addition, we considered the Nubia-ITRF08 angular velocity from DeMets *et al.* (2017) to assess the impact of a different reference frame in our kinematic modeling. The resulting Danakil–Nubia Euler pole (16.32°N, 40.06°E, 2.83 deg Myr^{-1}) falls within the error ellipse of the solution using the Altamimi *et al.* (2012) reference (Table 2), confirming the robustness of our estimation. This alternative reference frame test was also applied for the inter-rifting deformation modeling (next section), for which similar results were obtained.

We tested the significance of the decrease in χ^2 by Model 3 relative to Models 1 and 2 by means of the F-ratio test described in Stein & Gordon (1984). From the set of 14 GPS velocities along the entire Danakil block, F-ratios of 17.8 and 17.0 were obtained, respectively. Both estimates are higher than the $f_{0.001}$ critical value (7.8) at 99.9 per cent confidence level, supporting our new Model 3 with a significantly smaller Danakil microplate than previously suggested (Varet 2018).

6 INTER-RIFTING DEFORMATION IN GULF OF ZULA

The Gulf of Zula is characterized by recent tectonic structures (∼1 Ma) in the area forming two left-stepping grabens, where the east–west oriented extension associated with the Danakil–Nubia relative motion is accommodated (Sani *et al.* 2017, fig. 6). Given the absence of significant volcano-tectonic events in the area during the time span of our measurements and in the historical archives, the steady-state component of deformation is well represented by our GPS velocity field. The clear velocity gradient of GPS stations across the gulf confirms extensional motions in the area (Figs 2 and 6) and indicates a rather diffuse deformation pattern at this part of the Danakil–Nubia boundary (e.g., Garfunkel & Beyth 2006, fig. 6). The GPS velocities, after correcting for the Danakil–Nubia relative block motion (Model 3, Table 2, Fig. 6) and projected along a ∼N84°E profile (Fig. 7), suggest a typical inter-rifting signal, similar to what has been observed in Afar and Iceland (e.g. Smittarello *et al.* 2016; Drouin *et al.* 2016).

We assess the spatial distribution of active deformation in the Gulf of Zula area by means of a 1-D arctangent model, modified after Savage & Burford (1973) for the case of divergent plate boundaries. In this model, the velocity component into the spreading direction $V_{sp}(x)$ at any location x on a profile crossing the boundary can be expressed as a function of the full plate relative velocity V_r and the effective plate-boundary locking depth D (modified after Heimisson *et al.* 2015):

$$V_{sp} = a_0 + \frac{V_r}{\pi} \times arctan\left[\frac{(x - s)}{D}\right] \qquad (1)$$

with parameters a_0 and s allowing for a reference frame adjustment and a shift in the centre location of the plate boundary, respectively. This elastic inter-rifting model has been successfully applied in describing the horizontal velocity field at the plate boundary in Iceland (e.g. Islam & Sturkell 2015; Drouin *et al.* 2016), while an equivalent approach has been implemented for magmatic segments within Afar (e.g. Smittarello *et al.* 2016).

After removing the rotational velocity component from GPS stations on the Danakil block (Model 3, Table 2), the velocity vectors were projected into the N84°E direction, roughly parallel to the mean strike orientation of tectonic structures in the area (e.g. Sani *et al.* 2017, Figs 6 and 7). The predicted steady-state Danakil–Nubia

Table 2. Euler poles, angular velocities and uncertainties for the motion of the Danakil block relative to neighboring tectonic plates derived from our kinematic models.

[Model]Plate pair	(°)		(deg Myr^{-1})				Covariance matrix[a] ($\times 10^{-3}$)					
	Lat.	Lon.	ω_x	ω_y	ω_z	$\|\omega\|$	σ_x^2	σ_y^2	σ_z^2	σ_{xy}	σ_{xz}	σ_{xz}
[1]Danakil-Nubia	17.00	39.70	1.398	1.161	0.555	1.90	10.66	32.39	46.95	-16.76	-16.00	28.23
[2]Danakil-Nubia	16.62	39.73	1.693	1.407	0.657	2.30	0.82	0.64	0.09	0.72	0.27	0.24
[3]Danakil-Nubia	16.36	39.96	2.082	1.744	0.797	2.83	2.67	1.99	0.32	2.30	0.92	0.80
[3]Danakil-Arabia	13.80	41.92	1.774	1.593	0.586	2.45	3.19	2.76	0.63	2.93	1.32	1.28
[3]Danakil-Somalia	15.08	39.96	2.131	1.785	0.749	2.88	2.74	2.06	0.34	2.36	0.91	0.78
[3]Danakil-ITRF08[b]	20.76	36.82	2.108	1.578	0.998	2.82	2.68	1.99	0.32	2.30	0.92	0.79

[a]Elements of the angular velocity covariance matrix have units of (deg Myr^{-1})^2, [b] describes the motion of the Danakil block relative to the ITRF08, constrained after the Altamimi *et al.* (2012) plate motion model.
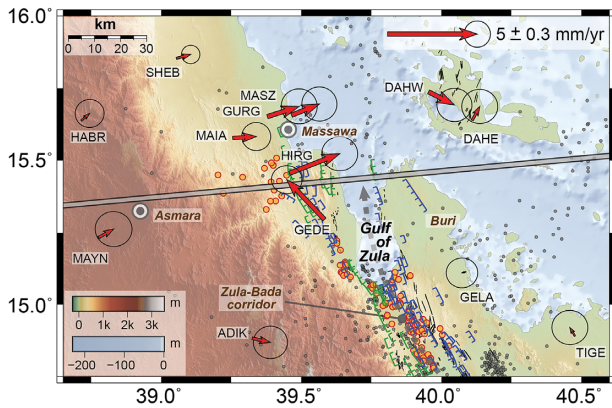

Figure 6. Fault locations, volcanic vents (orange circles) and local seismicity (grey dots) during 2011–2013 of the Gulf of Zula area (after Illsley-Kemp *et al.* 2018) along with horizontal GPS velocities (red arrows with 95 per cent confidence ellipses) after removing the steady-state rotation of the Danakil block from stations located east of HIRG. East-dipping normal faults are shown in green and west-dipping faults in blue (Sani *et al.* 2017), with additional tectonic structures shown as solid black lines. The thick grey line marks a profile parallel to the mean strike orientation of tectonic structures in the area (after Sani *et al.* 2017) and used for Fig. 7.

velocities change somewhat within the study area, due to the proximity of the Danakil–Nubia Euler pole (Fig. 5), and we thus used an average opening-rate value from Model 3 of $V_r = 5.6$ mm yr^{-1} in the inter-rifting deformation modeling. Parameter a_0 was introduced to correct for the small residual velocities observed at the far-field stations (e.g. ADER, HABR) with respect to the Nubian-fixed reference frame. From V_{sp} in eq. (1), we also subtract a Heaviside-step function term $H(x - s)$ of amplitude V_r to account for the rigid block motion that has already been removed from stations on the Danakil block. Finally, a weighted non-linear least-squares optimization was used to find model parameters a_0, s and D and their associated covariance matrix.

This modeling yields an effective locking depth of $D = 12 + 3$ km and locates the Danakil–Nubia centre of deformation about 10 km west of the Gulf of Zula coast (i.e. GPS station GEDE falls within the Danakil block, Figs 6 and 7). Similar values of D have been estimated for the Eastern and Northern volcanic zones of Iceland (e.g. Islam & Sturkell 2015; Drouin *et al.* 2016), consistent with the anomalously thick and elevated crust beneath both Afar and Iceland (Wright *et al.* 2012). The high effective locking depth results from the large width of the inter-rifting deformation zone, with ∼90 per cent of the deformation taking place within ±75 km distance from the plate boundary (Fig. 7). In northern Afar, such

broad regions of distributed deformation have been found to characterize areas where mechanical extension is dominant over magma assisted extension (e.g. Bastow *et al.* 2018), with faulting in the upper crust and ductile flow in the lower crust being the main deformation drivers (Bastow & Keir 2011; Ebinger *et al.* 2017). The modeling provides first-order constraints on the distribution of active deformation in the Gulf of Zula area without accounting for possible local complexities within the deformation field (e.g. Ghebreab & Talbot 2000; Sani *et al.* 2017). Associating the deformation with individual faults or other structures would require observations at more sites. Nevertheless, the results show that the inter-rifting deformation is not focused in the gulf itself (Fig. 7). The presence of volcanic vents and distributed faults to the west of Zula further support this model results (e.g. Sani *et al.* 2017, fig. 6).

7 DISCUSSION

Our geodetic observations and modeling confirm the present-day coherent rotation of the Danakil block between the southern Red Sea and Danakil-Afar rifts. However, the size of the block appears to be smaller than in earlier models, with the southernmost Red Sea and eastern Afar being parts of the Arabian plate (Vigny *et al.* 2006; Varet 2018, Fig. 5 and Table 2). This result is further supported by the lack of evidence for an active plate boundary south of Hanish-Zukur Islands, that is the GPS velocity field shows no opening south of the islands, the Bab-el-Mandeb Strait appears to be seismically inactive, with no record of moderate or strong earthquakes in the instrumental seismicity archives (e.g. Hofstetter & Beyth 2003; Varet 2018; ISC 2019), and there are no morphological or volcanological expressions of the rift axis extending this far south (Schettino *et al.* 2016; Almalki *et al.* 2016). Furthermore, vent alignments, crater elongations and eruptive fissure and/or volcanic ridge orientations in and around the Hanish-Zukur Islands and the Nabro-Dubbi volcanoes (N40°E, Fig. 4) suggest a possible en echelon plate boundary connecting the two rift branches within Afar.

The northward migration of the Danakil-Nubia Euler vector (∼200 km during recent geological times, McClusky *et al.* 2010; Reilinger & McClusky 2011) and the stability of the Afar eastern margins during the last ∼8 Ma (Varet 2018) are also consistent with the addition of the southernmost Danakil block to the Arabian plate. However, the boundary of the Danakil block at this location, extending from the Hanish-Zukur Islands into Afar, is not well defined. Our modeling primarily suggests shear motion along this boundary (Fig. 5), not directly supporting its likely 'leaky' nature (Barberi & Varet 1977; Courtillot 1982), evident by the extensive volcanism (Fig. 4). Further west Model 3 even predicts transpressional motion within Afar, contrasting with extensional features observed in the
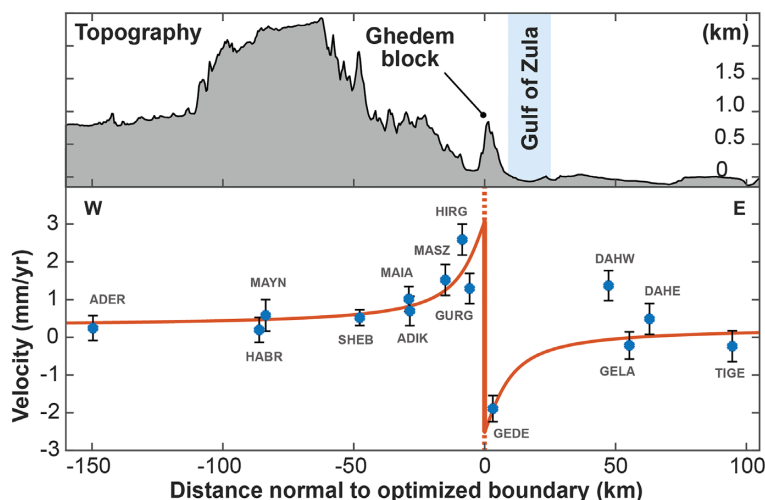
Figure 7. GPS velocities (blue circles with 1σ bars) in the ∼N84°E direction (see Fig. 6) after the Danakil–Nubia relative block motion has been removed, in comparison to the best-fitting inter-rifting model prediction (solid red line) and the profile topography (top).

area (e.g. Doubre *et al.* 2017; Polun *et al.* 2018; Pagli *et al.* 2019; La Rosa *et al.* 2019). GPS observations from a denser geodetic network would allow for more accurate strain quantification in the area, and therefore, provide further constraints on the block boundary location.

Looking at the other parts of the Danakil block boundary, the current GPS velocity field in the Gulf of Zula area is dominated by broad inter-rifting deformation extending ∼75 km away from the plate boundary (Figs 6 and 7). Similarities with other areas in northern Afar (e.g. Bastow *et al.* 2018), suggest that mechanical extension is dominant over magma assisted deformation around the gulf. Tectonic structures in the area (e.g. Drury *et al.* 1994; Ghebreab & Talbot 2000; Sani *et al.* 2017, Fig. 6) show similar horsetail terminations as seen at other rift segments within Afar (e.g. Manighetti *et al.* 2001b, 2009, 2015), supporting distributed deformation away from the main rift-bounding faults (Perrin *et al.* 2016). In line with the latter observation, we determine the centre location of the spreading boundary ∼10 km west of the Gulf of Zula shoreline (Figs 6 and 7). The optimal boundary location correlates well with a NNW–SSE sediment-filled graben bordered by normal faults of opposite dip orientation (e.g. Sani *et al.* 2017), located between the Ghedem block to the east and the basement units to the west (e.g. Drury *et al.* 1994, Figs 6 and 7). This suggests that the active deformation may be gradually moving west away from the Zula-Bada corridor (Frazier 1970, Fig. 6) and/or shifting between tectonic structures during different inter-rifting periods (Metzger & Jónsson 2014). Note that the city of Massawa, that has been destroyed several times in the past (e.g. 1884, 1921) by earthquake swarms (Gouin 1979), is located near our proposed boundary. The relatively thick seismogenic layer estimated for this part of the Danakil–Nubia plate boundary (12 ± 3 km) is also consistent with the crust beneath the Danakil Depression being 5–10 km thicker than normal oceanic crust (e.g. Hammond *et al.* 2011; Ebinger *et al.* 2017) and thus resulting in more diffuse inter-rifting deformation.

The rotation parameters of our preferred Model 3 predict left-lateral strike-slip motion at the northernmost edge of the Danakil block, with increasing transpression towards the Red Sea rift (Fig. 5). The transform motion is consistent with earthquake focal mechanisms in this area, which have been interpreted as occurring on north–south oriented sinistral strike-slip faults (Chu & Gordon

1998). The small magnitude of the shear conjointly with the presence of thick evaporite deposits (∼4 km around the Dahlak islands, Carbone *et al.* 1998) correlate well with the moderate seismicity and the lack of well-developed tectonic structures and/or tectonically driven seafloor topography (Varet 2018). Yet, our block boundary in this area is rather speculative since the tectonic structures connecting the Red Sea and Danakil-Afar rifts are still unknown (Varet 2018).

8 CONCLUSIONS

Combining up to 16 yr of GNSS observations for an improved velocity field of the southern Red Sea, Afar and Gulf of Aden region has allowed us to determine an updated kinematic block model for the entire study area. The velocity field reveals the diffuse character of the Danakil–Nubia plate boundary in Gulf of Zula, where inter-rifting deformation extends over more than 100-km-wide deformation zone. Our results also suggest that the Danakil block is significantly smaller than previously reported and only extending south to the Hanish-Zukur Islands in the southern Red Sea. GPS velocities on the northern part of the block show a coherent rotation relative to the Nubian plate about the Euler pole located at 16.36°N, 39.96°E and rotating at 2.83 deg Myr^{-1}. South of the of Hanish-Zukur Islands, on the other hand, the GPS velocities are better described by the Arabia–Nubia relative motion, supporting the addition of the southernmost part of Eritrea and northern Djibouti to the Arabian plate.

REFERENCES

Acton, G.D., Stein, S. & Engeln, J.F., 1991. Block rotation and continental extension in Afar: a comparison to oceanic microplate systems, *Tectonics,* **3**, 501–526.

Ahmed, A. *et al.*, 2016. Seafloor spreading event in western Gulf of Aden during the November 2010-March 2011 period captured by regional seismic networks: evidence for diking events and interactions with a nascent transform zone, *Geophys. J. Int.,* **205**, 1244–1266.

Al-Amri, A.M.S., Punsalan, B.T. & Uy, E.A., 1998. Spatial distribution of the seismicity parameters in the Red Sea regions, *J. Asian Earth Sci.,* **16**, 557–563.

Almalki, K.A., Betts, P.G. & Ailleres, L., 2016. Incipient seafloor spreading segments: Insights from the Red Sea, *Geophys. Res. Lett.,* **43**, 2709–2715.

Altamimi, Z., Métivier, L. & Collilieux, X., 2012. ITRF2008 plate motion model, *J. geophys. Res.,* **117**, B07402, doi:10.1029/2011JB008930.

Altamimi, Z., Métivier, L., Rebischung, P., Rouby, H. & Collilieux, X., 2017. ITRF2014 plate motion model, *Geophys. J. Int.,* **209**, 1906–1912.

Anderson-Fontana, S., Engeln, J.F., Lundgren, P., Larson, R.L. & Stein, S., 1986. Tectonics and evolution of the Juan Fernandez Microplate at the Pacific-Nazca-Antarctic Triple Junction, *J. geophys. Res.,* **91**, 2005–2018.

ArRajehi, A. *et al.*, 2010. Geodetic constraints on present-day motion of the Arabian Plate: implications for Red Sea and Gulf of Aden rifting, *Tectonics,* **29**, TC3011, doi:10.1029/2009TC002482.

ArRajehi, A., Zahran, H. & Reilinger, R., 2013. *Saudi Arabia 2013, GPS/GNSS Observations Dataset,* UNAVCO, doi:10.7283/W8X6-YT86.

Barberi, F. & Varet, J., 1977. Volcanism of Afar: small-scale plate tectonics implications, *Bull. geol. Soc. Am.,* **88**, 1251–1266.

Bastow, I.D. & Keir, D., 2011. The protracted development of the continent-ocean transition in Afar, *Nat. Geosci.,* **4**, 248–250.

Bastow, I.D. *et al.*, 2018. The development of late-stage continental breakup: seismic reflection and borehole evidence from the Danakil Depression, Ethiopia, *Tectonics,* **37**, 2848–2862.

Beyth, M., 1991. "Smooth" and "rough" propagation of spreading Southern Red Sea-Afar depression, *J. African Earth Sci.,* **13**, 157–171.

Bird, P., 2003. An updated digital model of plate boundaries, *Geochem. Geophys. Geosyst.,* **111**(4), 1027, doi:10.1029/2001GC000252.

Bosworth, W., 2015. *Geological Evolution of the Red Sea: Historical Background, Review and Synthesis. In: The Red Sea,* 45–78, doi:10.1007/978-3-662-45201-1_3.

Carbone, F., Matteucci, R. & Angelucci, A., 1998. *Present-day Sedimentation on the Carbonate Platform of the Dahlak Islands, Eritrea (inbook),* Springer Netherlands, pp. 523–536, doi:10.1007/978-94-011-4930-3_28.

Chu, D. & Gordon, R.G., 1998. Current plate motions across the Red Sea, *Geophys. J. Int.,* **135**, 313–328.

Cochran, J., 1983. A Model for Development of Red Sea, *Am. Assoc. Petrol. Geol. Bull.,* **67**, 41–69.

Collet, B., Taud, H., Parrot, J.F., Bonavia, F. & Chorowicz, J., 2000. A new kinematic approach for the Danakil block using a Digital Elevation Model representation, *Tectonophysics,* **316**, 343–357.

Consiglio Nazionale delle Ricerche (CNR) and Centre National de la Recherche Scientifique(CNRS), 1975. *Geological Map of Afar, 2, Central and Southern Afar,* Geotechnip, La Celle St. Cloud, France, scale 1:500000.

Courtillot, V., 1980. Opening of the gulf of Aden and Afar by progressive tearing, *Phys. Earth planet. Inter.,* **21**, 343–350.

Courtillot, V., 1982. Propagating rifts and continental breakup, *Tectonics,* **3**, 239–250.

Courtillot, V., Achache, J., Landre, F., Bonhommet, N., Montigny, R. & Féraud, G., 1984. Episodic spreading and rift propagation: New paleomagnetic and geochronologic data from the Afar Nascent passive margin, *J. geophys. Res.,* **89**, 3315–3333.

Courtillot, V., Armijo, R. & Tapponnier, P., 1987. Kinematics of the Sinai triple junction and a two-phase model of Arabia-Africa rifting, *Geol. Soc. Lond. Spec. Publ.,* **28**, 559–573.

DeMets, C., Calais, E. & Merkouriev, S., 2017. Reconciling geodetic and geological estimates of recent plate motion across the Southwest Indian Ridge, *Geophys. J. Int.,* **208**, 118–133.

Doubre, C. *et al.*, 2016. Current deformation in Central Afar and triple junction kinematics deduced from GPS and InSAR measurements, *Geophys. J. Int.,* **208**, 936–953.

Drouin, V., Sigmundsson, F., Ófeigsson, B.G., Hreinsdóttir, S., Sturkell, E. & Einarsson, P., 2017. Deformation in the Northern Volcanic Zone of Iceland 2008–2014: an interplay of tectonic, magmatic, and glacial isostatic deformation, *J. geophys. Res.,* **122**, 158–3178.

Drury, S.A., Kelley, S.P., Berhe, S.M., Collier, R.E. L. & Abraha, M., 1994. Structures related to Red Sea evolution in northern Eritrea, *Tectonics,* **13**, 1371–1380.

Eagles, G., Gloaguen, R. & Ebinger, C., 2002. Kinematics of the Danakil microplate, *Earth planet. Sci. Lett.,* **203**, 607–620.

Ebinger, C.J. & Hayward, N.J., 1996. Soft plates and hot spots: Views from Afar, *J. geophys. Res.,* **101**, 21 859–21 876.

Ebinger, C., Ayele, A., Keir, D., Rowland, J., Yirgu, G., Wright, T., Belachew, M. & Hamling, I., 2010. Length and Timescales of Rift Faulting and Magma Intrusion: the Afar Rifting Cycle from 2005 to Present, *Ann. Rev. Earth planet. Sci.,* **38**, 439–466.

Ebinger, C.J. *et al.*, 2017. Crustal structure of active deformation zones in Africa: implications for global crustal processes, *Tectonics,* **36**, 3298–3332.

Engeln, J.F., Stein, S., Werner, J. & Gordon, R.G., 1988. Microplate and shear zone models for oceanic spreading center reorganizations, *J. geophys. Res.,* **93**, 2839–2856.

Floyd, M.A. *et al.*, 2010. A new velocity field for Greece: implications for the kinematics and dynamics of the Aegean, *J. geophys. Res.,* **115**, B10403, doi:10.1029/2009JB007040.

Frazier, S.B., 1970. Adjacent structures of Ethiopia: that portion of the Red Sea Coast Including Dahlak Kebir Island and the Gulf of Zula, *Phil. Trans. R. Soc. Lond., A,* **267**, 131–141.

Garfunkel, Z. & Beyth, M., 2006. Constraints on the structural development of Afar imposed by the kinematics of the major surrounding plates, *Geol. Soc., Lond., Spec. Publ.,* **259**, 23–42.

Gass, I.G., Mallick, D.I.J. & Cox, K.G., 1973. Volcanic islands of the Red Sea, *J. Geol. Soc.,* **129**, 275–309.

Ghebreab, W. & Talbot, C.J., 2000. Red Sea extension influenced by Pan-African tectonic grain in eastern Eritrea, *J. Struct. Geol.,* **22**, 931–946.

Ghebreab, W., Ogubazghi, G. & Reilinger, R., 2010a. *Eritrea 2004, GPS/GNSS Observations Dataset,* UNAVCO, doi:10.7283/PZWB-S106.

Ghebreab, W., Ogubazghi, G. & Reilinger, R., 2010b. *Eritrea 2005, GPS/GNSS Observations Dataset,* UNAVCO, doi:10.7283/HWEW-8B62.

Goitom, B. *et al.*, 2015. First recorded eruption of Nabro volcano, Eritrea, 2011, *Bull. Volcanol.,* **77**, 1–21.

Gouin, P., 1979. *Earthquake History of Ethiopia and the Horn of Africa,* International Development Research Centre, Ottawa.

Grandin, R. *et al.*, 2009. September 2005 Manda Hararo-Dabbahu rifting event, Afar (Ethiopia): constraints provided by geodetic data, *J. geophys. Res.,* **114**, B08404, doi:10.1029/2008JB005843.

Guidarelli, M., Stuart, G., Hammond, J.O.S., Kendall, J.M., Ayele, A. & Belachew, M., 2011. Surface wave tomography across Afar, Ethiopia: Crustal structure at a rift triple-junction zone, *Geophys. Res. Lett.,* **38**, L24313, doi:10.1029/2011GL046840.

Hamling, I.J., Wright, T.J., Calais, E., Bennati, L. & Lewi, E., 2010. Stress transfer between thirteen successive dyke intrusions in Ethiopia, *Nat. Geosci.,* **3**, 713–717.

Hamlyn, J.E. *et al.*, 2014. Seismicity and subsidence following the 2011 Nabro eruption, Eritrea: insights into the plumbing system of an off-rift volcano, *J. geophys. Res.,* **119**, 8267–8282.

Hammond, J.O.S., Kendall, J.-M., Stuart, G.W., Keir, D., Ebinger, C., Ayele, A. & Belachew, M., 2011. The nature of the crust beneath the Afar triple junction: evidence from receiver functions, *Geochem. Geophys. Geosyst.,* **12**, Q12004, doi:10.1029/2011GC003738.

Hammond, J.O.S., Kendall, J.-M., Wookey, J., Stuart, G.W., Keir, D. & Ayele, A., 2014. Differentiating flow, melt, or fossil seismic anisotropy beneath Ethiopia, *Geochem. Geophys. Geosyst,* **15**, 1878–1894.

Hayward, N.J. & Ebinger, C.J., 1996. Variations in the along-axis segmentation of the Afar Rift system, *Tectonics,* **15**, 244–257.

Heimisson, E.R., Hooper, A. & Sigmundsson, F., 2015. Forecasting the path of a laterally propagating dike, *J. geophys. Res.,* **120,** 8774–8792.

Herring, T.A., King, R.W., Floyd, M.A. & McClusky, S.C., 2015. *Documentation for the GAMIT/GLOBK GPS software analysis, release 10.6,* Massachusetts Institute of Technology Cambridge.

Hofstetter, R. & Beyth, M., 2003. The Afar depression: interpretation of the 1960–2000 earthquakes, *J. geophys. Int.,* **155,** 715–732.

Illsley-Kemp, F. *et al.*, 2018. Seismicity during continental breakup in the Red Sea rift of Northern Afar, *J. geophys. Res.,* **123,** 2345–2362.

International Seismological Centre, 2019. *On-line Bulletin,* doi:10.31905/D808B830.

Islam, Md.T. & Sturkell, E., 2015. Temperature-dependent newtonian rheology in advection-convection geodynamical model for plate spreading in eastern volcanic zone, Iceland, *J. Geosci. Environ. Prot.,* **3,** 14–26.

Joffe, S. & Garfunkel, Z., 1987. Plate kinematics of the circum Red Sea-a re-evaluation, *Tectonophysics,* **141,** 5–22.

Keir, D., Bastow, I.D., Pagli, C. & Chambers, E.L., 2013. The development of extension and magmatism in the Red Sea rift of Afar, *Tectonophysics,* **607,** 98–114.

Kogan, L., Fisseha, S., Bendick, R., Reilinger, R., McClusky, S., King, R. & Solomon, T., 2012. Lithospheric strength and strain localization in continental extension from observations of the East African Rift, *J. geophys. Res.,* **117,** B03402, doi:10.1029/2011JB008516.

La Rosa, A., Pagli, C., Keir, D., Sani, F., Corti, G., Wang, H. & Possee, D., 2019. Observing oblique slip during rift linkage in northern Afar, *Geophys. Res. Lett.,* **46,** 10 782–10 790.

Le Pichon, X. & Francheteau, J., 1978. A plate-tectonic analysis of the Red Sea-Gulf of Aden Area, *Tectonophysics,* **46,** 369–388.

Makris, J. & Ginzburg, A., 1987. The Afar depression: transition between continental rifting and sea-floor spreading, *Tectonophysics,* **141,** 199–214.

Manighetti, I., Tapponnier, P., Courtillot, V., Gruszow, S. & Gillot, P.-Y., 1997. Propagation of rifting along the Arabia-Somalia Plate boundary: the Gulfs of Aden and Tadjoura, *J. geophys. Res,* **102**(B2), 2681–2710.

Manighetti, I., Tapponier, P., Gillot, P.Y., Jacques, E., Courtillot, V., Armijo, R., Ruegg, J.C. & King, G., 1998. Propagation of rifting along the Arabia-Somalia Plate Boundary: into Afar, *J. geophys. Res.,* **103**(B3), 4947–4974.

Manighetti, I., Tapponnier, P., Courtillot, V., Gallet, Y., Jacques, E. & Gillot, P.Y., 2001a. Strain transfer between disconnected, propagating rifts in Afar, *J. geophys. Res.,* **106,** 13 613–13 665.

Manighetti, I., King, G.C.P., Gaudemer, Y., Scholz, C.H. & Doubre, C., 2001b. Slip accumulation and lateral propagation of active normal faults in Afar, *J. geophys. Res.,* **106,** 13 667–13 696.

Manighetti, I., Zigone, D., Campillo, M. & Cotton, F., 2009. Self-similarity of the largest-scale segmentation of the faults: Implications for earthquake behavior, *Earth planet. Sci. Lett.,* **288,** 370–381.

Manighetti, I., Caulet, C., Barros, L.D., Perrin, C., Cappa, F. & Gaudemer, Y., 2015. Generic along-strike segmentation of Afar normal faults, East Africa: implications on fault growth and stress heterogeneity on seismogenic fault planes, *Geochem. Geophys. Geosyst.,* **16,** 443–467.

Maus, S. *et al.*, 2009. EMAG2: a 2-arc min resolution Earth Magnetic Anomaly Grid compiled from satellite, airborne, and marine magnetic measurements, *Geochem. Geophys. Geosyst.,* **10,** Q08005, doi:10.1029/2009GC002471.

McCaffrey, R., 1995. *DEFNODE Users' Guide,* Rensselaer Polytech. Inst.

McCaffrey, R., 2002. Crustal block rotations and plate coupling, in *Plate Bound. Zones,* Vol. **30,** pp. 101–122, eds Stein, S. & Freymueller, J., doi:10.1029/GD030p0101.

McCaffrey, R., 2009. Time-dependent inversion of three-component continuous GPS for steady and transient sources in northern Cascadia, *Geophys. Res. Lett.,* **36,** L07304, doi:10.1029/2008GL036784.

McClusky, S. *et al.*, 2010. Kinematics of the southern Red Sea-Afar Triple Junction and implications for plate dynamics, *Geophys. Res. Lett.,* **37,** L05301, doi:10.1029/2009GL041127.

McKenzie, D.P., Davis, D. & Molnar, P., 1970. Plate tectonics of the Red Sea and East Africa, *Nature,* **226,** 243–248.

McQuarrie, N., Stock, J.M., Verdel, C. & Wernicke, B.P., 2003. Cenozoic evolution of Neotethys and implications for the causes of plate motions, *Geophys. Res. Lett.,* **30,** 2036, doi:10.1029/2003GL017992.

McQuarrie, N. & van Hinsbergen, D.J. J., 2013. Retrodeforming the Arabia-Eurasia collision zone: age of collision versus magnitude of continental subduction, *Geology,* **41,** 315–318.

Metzger, S. & Jónsson, S., 2014. Plate boundary deformation in North Iceland during 1992–2009 revealed by InSAR time-series analysis and GPS, *Tectonophysics,* **634,** 127–138.

Mohr, P.A., 1970. The Afar Triple Junction and sea-floor spreading, *J. geophys. Res.,* **75,** 7340–7352.

Nobile, A., Pagli, C., Keir, D., Wright, T.J., Ayele, A., Ruch, J. & Acocella, V., 2012. Dike-fault interaction during the 2004 Dallol intrusion at the northern edge of the Erta Ale Ridge (Afar, Ethiopia), *Geophys. Res. Lett.,* **39,** L19305, doi:10.1029/2012GL053152.

Ogubazghi, G. & Reilinger, R., 2010a. *Eritrea 2006, GPS/GNSS Observations Dataset,* UNAVCO, doi:10.7283/E34A-Y306.

Ogubazghi, G. & Reilinger, R., 2010b. *Eritrea 2007, GPS/GNSS Observations Dataset,* UNAVCO, doi:10.7283/ZRHT-6R81.

Ogubazghi, G. & Reilinger, R., 2010c. *Eritrea 2008, GPS/GNSS Observations Dataset,* UNAVCO, doi:10.7283/HSQ0-B809.

Ogubazghi, G. & Reilinger, R., 2010d. *Eritrea 2009, GPS/GNSS Observations Dataset,* UNAVCO, doi:10.7283/D284-FC97.

Pagli, C., Wright, T.J., Ebinger, C.J., Yun, S.-H., Cann, J.R., Barnie, T. & Ayele, A., 2012. Shallow axial magma chamber at the slow-spreading Erta Ale Ridge, *Nat. Geosci.,* **5,** 284–288.

Pagli, C., Wang, H., Wright, T.J., Calais, E. & Lewi, E., 2014. Current plate boundary deformation of the Afar rift from a 3-D velocity field inversion of InSAR and GPS, *J. geophys. Res.,* **119,** 8562–8575.

Pagli, C., Yun, S.-H., Ebinger, C., Keir, D. & Wang, H., 2019. Strike-slip tectonics during rift linkage, *Geology,* **47,** 31–34.

Perrin, C., Manighetti, I. & Gaudemer, Y., 2016. Off-fault tip splay networks: a genetic and generic property of faults indicative of their long-term propagation, *Comp. Rend. Geosci.,* **348,** 52–60.

Polun, S.G., Gomez, F. & Tesfaye, S., 2018. Scaling properties of normal faults in the central Afar, Ethiopia and Djibouti: implications for strain partitioning during the final stages of continental breakup, *J. Struct. Geol.,* **115,** 178–189.

Reilinger, R. & McClusky, S., 2011. Nubia-Arabia-Eurasia plate motions and the dynamics of Mediterranean and Middle East tectonics, *Geophys. J. Int.,* **186,** 971–979.

Sandwell, D.T., Müller, R.D., Smith, W.H. F., Garcia, E. & Francis, R., 2014. New global marine gravity model from CryoSat-2 and Jason-1 reveals buried tectonic structure, *Science,* **346,** 65–67.

Sani, F., Ghinassi, M., Papini, M., Oms, O. & Finotello, A., 2017. Evolution of the northern tip of Afar triangle: inferences from the quaternary succession of the Dandiero-Massawa area (Eritrea), *Tectonophysics,* **717,** 339–357.

Saria, E., Calais, E., Altamimi, Z., Willis, P. & Farah, H., 2013. A new velocity field for Africa from combined GPS and DORIS space geodetic solutions: contribution to the definition of the African reference frame (AFREF), *J. geophys. Res.,* **118,** 1677–1697.

Savage, J.C. & Burford, R.O., 1973. Geodetic determination of relative plate motion in central California, *J. geophys. Res.,* **78,** 832845.

Schettino, A., Macchiavelli, C., Pierantoni, P.P., Zanoni, D. & Rasul, N., 2016. Recent kinematics of the tectonic plates surrounding the Red Sea and Gulf of Aden, *Geophys. J. Int.,* **207,** 457–480.

Sichler, B., 1980. La biellette danakile: Un modéle pour l'évolution géodynamique de l'Afar, *Bull. Soc. Géol. Fr.,* **22,** 925–932.

Smittarello, D., Grandin, R., De Chabalier, J.-B., Doubre, C., Deprez, A., Masson, F., Socquet, A. & Saad, I.A., 2016. Transient deformation in the Asal-Ghoubbet Rift (Djibouti) since the 1978 diking event: is deformation controlled by magma supply rates? *J. geophys. Res.,* **121,** 6030–6052.

Souriot, T. & Brun, J.P., 1992. Faulting and block rotation in the Afar triangle, East Africa: the Danakil "crank-arm" model, *Geology,* **20,** 911–914.

Stab, M., Bellahsen, N., Pik, R., Quidelleur, X., Ayalew, D. & Leroy, S., 2016. Modes of rifting in magma-rich settings: tectono-magmatic evolution of Central Afar, *Tectonics,* **35,** 0278–7407.

Stein, S. & Gordon, R.G., 1984. Statistical tests of additional plate boundaries from platemotion inversions, *Earth planet. Sci. Lett.,* **69,** 401–412.

Tapponnier, P., Armijo, R., Manighetti, I. & Courtillot, V., 1990. Book-shelf faulting and horizontal block rotations between overlapping rifts in southern Afar, *Geophys. Res. Lett.,* **17,** doi:10.1029/GL017i001p00001.

Tazieff, H., Varet, J., Barberi, F. & Giglia, G., 1972. Tectonic significance of the Afar (or Danakil) depression, *Nature,* **235,** 144–147.

Varet, J., 2018. Transverse volcanic alignments along afar margins. in: geology of Afar (East Africa), in *Regional Geology Reviews*. Springer, pp. 241–251, doi:10.1007/978-3-319-60865-5_9.

Vigny, C., Huchon, P., Ruegg, J.C., Khanbari, K. & Asfaw, L.M., 2006. Confirmation of Arabia plate slow motion by new GPS data in Yemen, *J. geophys. Res.,* **111,** B02402, doi:10.1029/2004JB003229.

Vigny, C., de Chabalier, J.-B., Ruegg, J.-C., Huchon, P., Feigl, K.L., Cattin, R., Asfaw, L. & Kanbari, K., 2007. Twenty-five years of geodetic measurements along the Tadjoura-Asal rift system, Djibouti, East Africa, *J. geophys. Res.,* **112,** B06410, doi:10.1029/2004JB003230.

Wolfenden, E., Ebinger, C., Yirgu, G., Renne, P.R. & Kelley, S.P., 2005. Evolution of a volcanic rifted margin: southern Red Sea, Ethiopia, *Bull. geol. Soc. Am.,* **117,** 846–864.

Wright, T.J., Ebinger, C., Biggs, J., Ayele, A., Yirgu, G., Keir, D. & Stork, A., 2006. Magma-maintained rift segmentation at continental rupture in the 2005 Afar dyking episode, *Nature,* **442,** 291–294.

Wright, T. *et al.*, 2012. Geophysical constraints on the dynamics of spreading centres from rifting episodes on land, *Nat. Geosci.,* **5,** 242–250.

Xu, W. & Jónsson, S., 2014. The 2007-8 volcanic eruption on Jebel at Tair island (Red Sea) observed by satellite radar and optical images, *Bull. Volcanol.,* **76,** 795–808.

Xu, W., Ruch, J. & Jónsson, S., 2015. Birth of two volcanic islands in the southern Red Sea, *Nat. Commun.,* **6,** 7104–7110.

SUPPORTING INFORMATION

Supplementary data are available at *GJI* online.

Table S1: Horizontal GPS velocities with respect to the ITRF2008 (defined after Altamimi et al., 2012).

Please note: Oxford University Press is not responsible for the content or functionality of any supporting materials supplied by the authors. Any queries (other than missing material) should be directed to the corresponding author for the paper.